Eur. Phys. J. A (2014) **50**: 86
DOI 10.1140/epja/i2014-14086-9

THE EUROPEAN PHYSICAL JOURNAL A

Special Article – Experimental Physics

Energy measurement and fragment identification using digital signals from partially depleted Si detectors

for the FAZIA Collaboration

G. Pasquali[1,2,a], G. Pastore[1,2], N. Le Neindre[3], G. Ademard[4], S. Barlini[1,2], M. Bini[1,2], E. Bonnet[5], B. Borderie[4], R. Bougault[3], G. Casini[2], A. Chbihi[5], M. Cinausero[6], J.A. Dueñas[7], P. Edelbruck[4], J.D. Frankland[5], F. Gramegna[6], D. Gruyer[5], A. Kordyasz[8], T. Kozik[9], O. Lopez[3], T. Marchi[6], L. Morelli[10], A. Olmi[2], A. Ordine[11], M. Pârlog[3,12], S. Piantelli[2], G. Poggi[1,2], M.F. Rivet[4], E. Rosato[11,13], F. Salomon[4], G. Spadaccini[11,13], A.A. Stefanini[1,2], S. Valdrè[1,2], E. Vient[3], T. Twaróg[9], R. Alba[14], C. Maiolino[14], and D. Santonocito[14]

[1] Dipartimento di Fisica, Università di Firenze, via G. Sansone 1, 50019 Sesto Fiorentino (FI), Italy
[2] INFN, Sezione di Firenze, via G. Sansone 1, 50019 Sesto Fiorentino (FI), Italy
[3] LPC, IN2P3-CNRS, ENSICAEN et Université de Caen, F-14050 Caen-Cedex, France
[4] Institut de Physique Nucléaire, CNRS/IN2P3, Université Paris-Sud 11, F-91406 Orsay cedex, France
[5] GANIL, CEA/DSM-CNRS/IN2P3, B.P. 5027, F-14076 Caen cedex, France
[6] INFN-LNL Legnaro, viale dell'Università 2, 35020, Legnaro (Padova), Italy
[7] Departamento de Fisica Aplicada, FCCEE Universidad de Huelva, 21071 Huelva, Spain
[8] Heavy Ion Laboratory, University of Warsaw, ul. Pasteura 5a, 02-093 Warsaw, Poland
[9] Jagiellonian University, Institute of Nuclear Physics IFJ-PAN, PL-31342, Krakow, Poland
[10] INFN and Università di Bologna, 40126, Bologna, Italy
[11] INFN, Sezione di Napoli, 80126 Napoli, Italy
[12] "Horia Hulubei" National Institute of Physics and Nuclear Engineering, RO-077125 Bucharest, Romania
[13] Dipartimento di Fisica, Università di Napoli "Federico II", 80126 Napoli, Italy
[14] INFN-LNS Catania, 95129, Catania, Italy

Received: 14 February 2014 / Revised: 8 April 2014
Published online: 20 May 2014 –
Communicated by D. Pierroutsakou

Abstract. A study of identification properties of a Si-Si ΔE-E telescope exploiting an underdepleted residual-energy detector has been performed. Five different bias voltages have been used, one corresponding to full depletion, the others associated with a depleted layer ranging from 90% to 60% of the detector thickness. Fragment identification has been performed using either the ΔE-E technique or the Pulse Shape Analysis (PSA). Both detectors are reverse mounted: particles enter from the low field side, to enhance the PSA performance. The achieved charge and mass resolution has been quantitatively expressed using a Figure of Merit (FoM). Charge collection efficiency has been evaluated and the possibility of energy calibration corrections has been considered. We find that the ΔE-E performance is not affected by incomplete depletion even when only 60% of the wafer is depleted. Isotopic separation capability improves at lower bias voltages with respect to full depletion, though charge identification thresholds are higher than at full depletion. Good isotopic identification via PSA has been obtained from a partially depleted detector, whose doping uniformity is not good enough for isotopic identification at full depletion.

1 Introduction

In recent years, intensive experimental work has been devoted to improving the nuclear fragment identification techniques based on Pulse Shape (hereafter PS, PSA for PS Analysis) applied to Si detector signals. In fact, identification in mass (A) and charge (Z) of light charged particles and intermediate mass fragments will be particularly useful at Radioactive Ion Beam facilities for studies focused on nuclear isospin, where the N/Z ratio of the products will be a key experimental observable [1–4].

Large solid angle detector arrays usually feature a ΔE-E telescope as elemental cell [5–8]. A ΔE-E telescope is a multi-layer detection system: the impinging particle passes through the detectors one after the other and the energy deposited in each detector is measured [9]. However, neither fragments stopped in the first ΔE detector nor fragments punching through the whole telescope can

[a] e-mail: pasquali@fi.infn.it

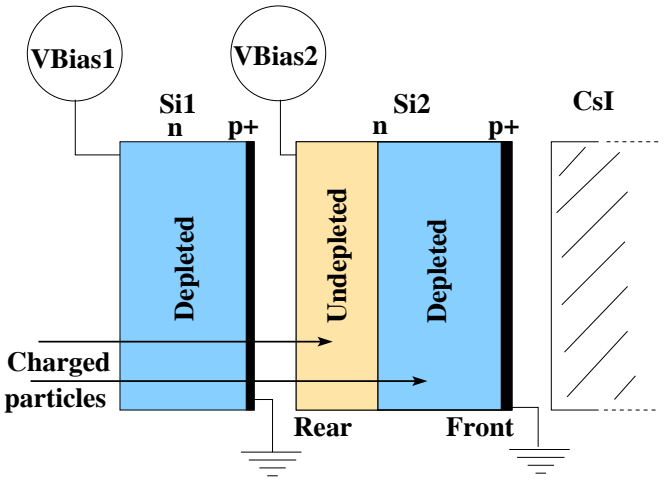

Fig. 1. (Color online) Sketch of the ΔE-E telescope employed in this work. Si detectors are mounted with the low field side facing the target (rear side injection). When Si2 is not fully depleted, particles enter the detector from the undepleted region. The picture is not to scale.

be uniquely identified. On the other hand, in a Si-Si-CsI telescope like those developed by the FAZIA Collaboration [10,11], PSA would allow identification of fragments stopped in the first Si detector, thus considerably lowering the energy threshold for identification.

Much has been learnt from previous tests of FAZIA telescope prototypes [12–15]. Other tests have been performed in the framework of the NUCL-EX Collaboration, exploiting the GARFIELD+RCo detector array at LNL [16]. An improvement of PSA isotopic identification capabilities in partially depleted Si detectors has been observed. A more systematic study of the PS identification capabilities of underdepleted Si detectors has thus been started. In a test performed at Laboratori Nazionali del Sud (LNS) of INFN, Si2, the second Si stage of a standard FAZIA telescope (see fig. 1), has been biased at five different bias voltages. One of the employed voltages corresponds to full depletion, the others are associated with depletion thicknesses ranging from 90% to 60% of the detector thickness. Though in a physics experiment one would obviously employ PSA on the first stage to lower the identification thresholds [13,14], studying the second stage is a school case which has many advantages. For instance, fragments stopped in the second stage can be identified with the ΔE-E technique exploiting the correlation between the charge collected from the two Si detectors. Knowing the fragment charge and mass, it is possible, *e.g.*, to estimate its incident energy from the ΔE energy deposited in the first stage, Si1. The energy value obtained from the calibration of the second stage can thus be cross-checked with the estimate based on the first one. PSA performance can also be better studied since charge and mass of the fragments stopped in Si2 are known from the ΔE-E correlation. The last statement also applies to partially depleted detectors since the quality of ΔE-E identification is unchanged (see sect. 3.2).

To improve PS identification capabilites, the Si detectors of FAZIA telescopes are mounted with the ohmic (low field) side facing the target [14]. Therefore, fragments enter a partially depleted detector from the undepleted region. In this work, we were interested in the following issues:

- What is the charge collection efficiency in the partially depleted detector for particles impinging on the undepleted region?
- Is the detector energy response linear with the deposited energy in such conditions?
- Is the ΔE-E identification affected by incomplete depletion of the detector?
- Is there really an improvement in PS identification?
- What are the energy thresholds for charge and mass identification?

A doping uniformity of about 1% FWHM, or less, would be needed to discriminate, *e.g.*, carbon isotopes via PSA in totally depleted detectors [12]. The doping uniformity of the detector under test is about 6%. It does not allow carbon isotopic identification via PSA at full depletion voltage (see sect. 3.5) but it does when it is underdepleted, even though in a reduced energy domain. A recent paper [17] showed that proton-deuteron separation at low energies improves when working near depletion voltage with respect to overdepletion. However, our work reports for the first time, as far as we know, about the possibility of improving the identification via PSA of fragments covering a relatively large range of charge and mass (and impinging energy) by underdepleting the silicon detector.

In sect. 2 the employed experimental setup is illustrated together with detector signal treatment. Section 3 discusses the performance achieved at the various bias voltages. In particular, sect. 3.1 presents the problem of charge amplitude estimation with the extremely slow signals coming from an underbiased detector, sect. 3.2 deals with the particle identification capabilites of the underdepleted detector using the usual ΔE-E technique in a telescope configuration. Section 3.3 deals with energy calibration using the so-called "punch-through" points. In sect. 3.4 the dependence of charge collection efficiency on the particle range is discussed. Finally, sect. 3.5 shows how fragment identification using PS identification methods depends on the applied bias voltage. Both the quality of charge and mass separation and the energy thresholds for identification are considered.

2 Experimental setup

The data presented in this work were collected in Catania at Laboratori Nazionali del Sud (LNS) of INFN. The beam was ^{84}Kr at 35 A MeV impinging on ^{112}Sn and ^{197}Au targets of thickness 488 μg/cm^2 and 178 μg/cm^2, respectively.

A telescope composed of Si 300 μm-Si 500 μm-CsI(Tl) 10 cm, was mounted in the "Ciclope" scattering chamber, at a distance from target of 50 cm and at $\approx 8^\circ$ polar angle with respect to the beam line, covering about 2° in

Table 1. Main features of the telescope employed in our test. The depletion voltage has been obtained from the C-V characteristics of the detectors. "Applied voltage" means the actual value applied to the silicon detector, taking into account the voltage drop on the bias resistor due to the leakage current. The full scale energy value takes into account the position of the signal baseline in the ADC range. Gain is given in keV/LSB units, where LSB is the Least Significant Bit of the ADC.

Technical Specs.	Si1	Si2	CsI(Tl)
Manufacturer	FBK	FBK	Amcrys
Bulk Type	n	n	
Thickness	311 μm	510 μm	10 cm + FBK diode
Active Area	$20 \times 20\,\mathrm{mm}^2$	$20 \times 20\,\mathrm{mm}^2$	$21 \times 21\,\mathrm{mm}^2$
Depletion Voltage	140 V	290 V	
Applied Voltage	140 V	105–290 V	30 V
Detector Capacitance	165 pF	160–100 pF	
Resistivity (Ω cm)	~ 2550	~ 2900	
Resistivity Uniformity (FWHM)	$\sim 4\%$	$\sim 6\%$	
Carrier Lifetime (μs)	6000	6000	
Digitizer (bit/rate)	14/100 MHz	14/100 MHz	12/125 MHz
Digitizer board ENOB	11.4	11.4	10
Energy Full Scale (Si-GeV)	3.7	2.5	0.4
P.A. Decay Const. (μs)	750	425	
Acquired signal length (μs)	20	70	30
Trapezoidal Shaper Rise Time (μs)	2	2	
Trapezoidal Shaper Flat Top (μs)	1	55	
Gain (keV/LSB)	283	192	

polar angle. A sketch of the telescope is shown in fig. 1 where two kinds of events are also depicted (arrows): particles stopped in the undepleted region of Si2 and particles reaching the depleted region.

The angular position of the telescope was slightly beyond the grazing angle, where the reaction mechanism concentrates most of the products (the grazing angle was $\sim 4.1^\circ$ and $\sim 6.0^\circ$ for ^{112}Sn and ^{197}Au targets, respectively). The same kind of telescope was employed in [14]. In table 1 we summarize the main characteristics of the telescope and of the dedicated front-end electronics (FEE). The detector thickness was measured via a precision gauge with an uncertainty of $\pm 1\mu$m and it was found to be 311 μm for Si1 and 510 μm for Si2. The detector capacitance as a function of the applied voltage was measured using a LCR Meter (HP 4332A): the measured values are such that the preamplifier risetime, as we have verified by bench tests, is not significantly affected by the capacitance variations due to changes of the applied voltage.

According to the usual FAZIA recipe for optimizing the PSA performance, both silicon detectors, manufactured by FBK (Trento, Italy) [18], were of the neutron transmutation doped (n-TD) type (for a better doping uniformity [12,19]) and cut at a "random" direction (to avoid "channeling" effects [12,20]). The mechanical mounting allowed us to use the Si detectors in transmission.

The voltage applied to the Si detectors was kept constant at the desired value using a bias system with reverse current monitoring that takes into account the voltage drop on the bias resistors of the preamplifiers (20 MΩ). However, no substantial correction was needed during data taking, since no increase in the reverse current (always less than 50 nA) has been noticed.

Table 2. Depletion depth, undepleted layer thickness, maximum rise-time and number of acquired signals at all employed bias voltages (see text).

Voltage on Si2 (V)	Depletion depth (μm)	Undepl. layer (μm)	Max. rise-time (20–70%) (μs)	Acquired signals ($\times 10^5$)
105	310	200	13	9
130	340	170	10	6
200	420	90	3.0	5
235	460	50	1.5	7
290	510	0	0.45	7

The bias voltage of Si1 has been kept at 140 V, full depletion value, during the whole measurement. Five different bias voltages have been applied to Si2, acquiring more than 5×10^5 events in each case. The number of events collected for each bias voltage is reported in table 2, rightmost column. Table 2 also reports the estimated depletion depth (obtained by scaling the value of full depletion with the square root of the ratio of the bias voltages) and maximum measured rise-time at all employed bias voltages (all rise-times quoted in this paper are taken from 20 to

70% of the maximum charge signal amplitude since this choice has been found to provide the best performances in terms of particle identification [12]). The estimate of the maximum rise-time reached at each bias voltage has been obtained from the "Energy *vs.* Charge rise-time" correlations (see, *e.g.*, sect. 3.5, fig. 6).

The Si detectors and the photodiode reading the CsI crystal where connected to PACI preamplifiers [21] placed under vacuum very close to the detectors. Signals were then brought outside vacuum using 8 m long differential cables, and connected to custom made digitizers. The digitizers for Si detectors, already used in all previous FAZIA tests, feature 14 bit ADC's with 100 MHz sampling rate. The effective number of bits (ENOB) of each digitizing board is about 11.4. Signals from the photodiode were sampled by a 12 bit/125 MHz digitizer [22].

In this work information coming from the CsI detector will be used only for vetoing particles not stopped in Si2 (punch-through particles). The CsI has a tapered shape well suited for a distance of 1 m from the target: at such a distance, particles passing through the Si detectors will be completely contained in the CsI in spite of their diverging paths. However, at the employed distance of 50 cm, particles impinging near the borders of the Si can escape the CsI. Therefore the CsI veto is not 100% efficient, as it will be clear from the ΔE-E and PSA correlations showed in figs. 3 and 6.

The acquired signal length for Si1 is 20 μs. For Si2, since charge collection times in an underdepleted detector can be more than an order of magnitude longer than at full depletion, the length of acquired signals has been set to 70 μs (*i.e.* 7000 samples, maximum length allowed by the FEE signal memory).

3 Data analysis

3.1 Amplitude measurement

For charge collection times of the order of 10 μs or more, the decay of the charge preamplifier signal (decay time constant $\approx$ 425 μs) and the associated ballistic deficit [23, 24] of the preamplifier signal (even before shaping) cannot be neglected (see fig. 2). Moreover, the ballistic deficit would depend on signal rise-times, varying greatly with the energy and the atomic number of the detected fragment, thus spoiling the energy resolution. To minimize this effect, a correction algorithm, including a pole-zero cancellation stage and an accumulator (*i.e.* an integrator), has been applied as part of the waveform shaping. The correction algorithm (*pole-zero correction* in the following) transforms an exponentially decaying signal with the time constant of the preamplifier into a step function. Figure 2, panel a), shows examples of the acquired preamplifier signal for Si2 at the lowest bias employed in the experiment (105 V). Signals refer to ^{18}F and ^{35}Cl ions. For each ion type, signals at two different energies are shown, after baseline subtraction [25]: the lower energy corresponding to an ion stopped in the undepleted region, the higher energy to an ion reaching the depleted region.

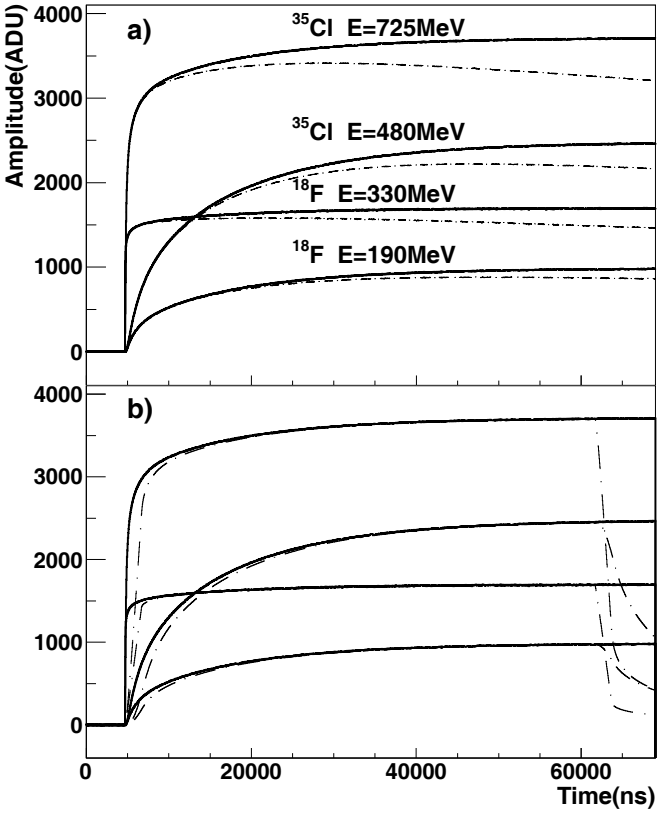

Fig. 2. Panel a): Digitized preamplifier signals in Si2 for ^{18}F at 190 and 330 MeV and for ^{35}Cl at 480 and 725 MeV. Each ion is stopped in the undepleted region at the lower energy and in the depleted region at the higher energy. The ranges associated with the two energies are 195 μm and 480 μm for ^{18}F, 190 μm and 360 μm for ^{35}Cl. For each energy, signals both with (full lines) and without pole-zero correction (dashed lines) are plotted. Panel b): Preamplifier signals, corrected with pole-zero correction before (full lines) and after (dashed lines) trapezoidal shaping with a very long ($>$ 50 μs) flat top. Data in both panels refer to the lowest employed bias voltage of 105 V.

The slow rise-time associated with the former, when compared to the latter, is apparent. Dashed and full lines show the shapes of the original signals and of the signals corrected for the finite preamplifier decay constant (pole-zero correction), respectively. For a given particle and energy, signals with and without correction are almost coincident during the leading edge, though their maximum amplitudes are substantially different. A ballistic deficit due to the finite preamplifier decay constant clearly appears as a reduction of a few % (about 10% for ^{35}Cl) in the maximum signal amplitude without correction.

After baseline subtraction and pole-zero correction the charge signal is shaped using a trapezoidal shaper algorithm. The shaper acts as a pass-band filter, with a bandwidth depending on the leading edge rise-time (fixed at 2 μs). The so-called "flat-top" length must be long enough to reduce ballistic deficit effects (*i.e.* the step response of the shaper must last long enough to accomodate the whole charge collection time). In fig. 2, panel b), the same preamplifier signals of panel a) with pole-zero correction applied

(full lines) are shown, together with the corresponding trapezoidally shaped signals (dashed lines). A quite long flat top of 55 μs has been used for Si2. For ions stopped in the undepleted region (slowest signals) it is clear that a shorter flat top of the trapezoidal shaper would produce a supplementary ballistic deficit. For those particles, the flat top of the shaper (which has unitary gain) would not last long enough to reach the maximum amplitude of the preamplifier, which occurs more than 50 μs after the leading edge.

On the other hand, a 1 μs long flat top is well suited for Si1 signals (not shown in fig. 2). The energy information is obtained from the maximum amplitude of the shaped signal. Numerical simulations of the behaviour of our trapezoidal shaper, employing realistic input signals, showed that the ballistic deficit with a 55 μs flat top is about 0.5% for the maximum measured rise-time ($\approx 13\,\mu$s, see table 2 and fig. 6) and less than 0.1% for rise-times $< 8\,\mu$s. Due to the relatively low gain of the preamplifier, noise fluctuations superimposed on the digitized signal are dominated by the digitizing noise which has an almost flat power spectrum: therefore, increasing the flat top length has no substantial effect on the electronic noise resolution.

3.2 ΔE-E identification

The ΔE-E technique allows for isotopic identification of fragments stopped in Si2. Already during data taking, a surprising agreement of the Si1-Si2 ΔE-E correlations at all applied bias voltages became apparent, possibly suggesting that the charge collection efficiency is almost independent (within few %) of the bias conditions (see sect. 3.3). Figure 3 shows, as an example, two ΔE-E correlations (Si1 *vs.* Si2) obtained at the highest (top panel) and lowest (bottom panel) bias voltages applied to Si2. No degradation of the isotopic separation can be spotted in the figure, though at 105 V Si2 is only depleted by 60%.

A linearization procedure based on identification curves manually drawn on the ridges of the ΔE-E correlation allows for extraction of the so-called Particle IDentification (PID) parameter. Intervals of PID are then assigned to a definite (Z, A) pair. The assignment of the correct (Z, A) pair to a given ΔE-E ridge is mainly a matter of self-consistency. The Z value can be easily derived just by counting the ridges in the ΔE-E correlation (the $Z = 4$ lines are easily recognized since ^{8}Be decays before reaching the detector, leaving a gap between ^{7}Be and ^{9}Be). The mass assignment is an easy task for the lighest fragments with $Z \leq 4$. For $Z > 4$ a wrong mass value assigned to one of the isotopes employed in the calibrations (see sect. 3.3) would produce a sizeable increase of the χ^2 of the calibration fit reported in table 4. Mass values are assigned first to the isotopes employed for calibrations at 290 V. The stability of the ΔE-E correlation with applied voltage guarantees that the same assignements are also valid at the other voltages. Extension to other isotopes, not employed for calibration, is obtained by comparing the experimental ΔE-E correlation, after energy calibration, with the estimates of the energy loss

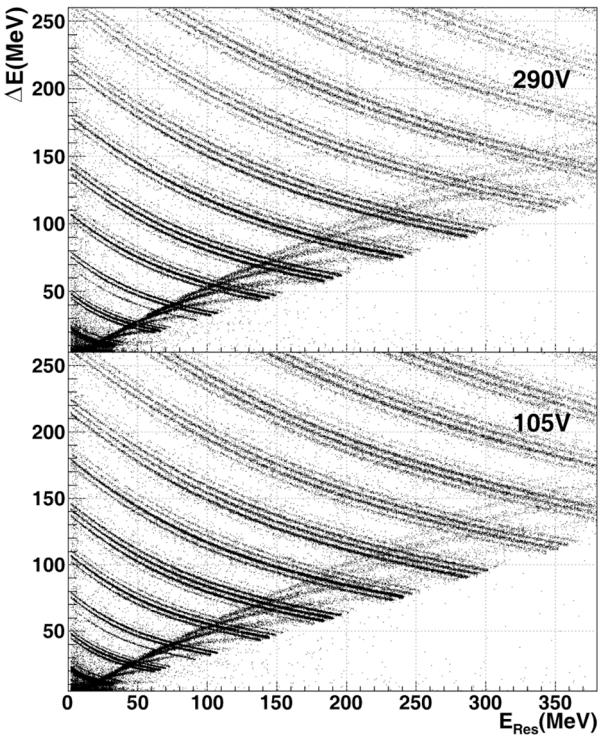

Fig. 3. Top: ΔE-E correlation "Si1 *vs.* Si2" at a 290 V bias voltage. Bottom: The same ΔE-E correlation at a 105 V bias voltage. Particles punching-through Si2 are excluded using the CsI information: however, a residual contamination by such events is still present due to geometrical reasons (see sect. 2).

calculations. Figure 4 illustrates the good agreement between experimental data and energy loss estimates: the full lines are the interpolation lines manually drawn on top of the experimental ridges in the framework of the linearization procedure. The dashed lines are obtained from energy loss calculations exploiting the range-energy tables of [26].

As in previous FAZIA experiments (see, *e.g.*, ref. [13]), the "Figure of Merit" (FoM) has been employed in order to quantitatively express the obtained discrimination power. From the PID spectrum, the FoM [27] for adjacent isotopes is defined as

$$\mathrm{FoM} = \frac{|\overline{\mathrm{PID}_1} - \overline{\mathrm{PID}_2}|}{\mathrm{FWHM}_1 + \mathrm{FWHM}_2}\,, \qquad (1)$$

where $\overline{\mathrm{PID}_1}$ and $\overline{\mathrm{PID}_2}$ are the centroids of the peaks associated to two neighboring isotopes and FWHM_1 and FWHM_2 are their full widths at half maximum. Table 3 reports FoM values, integrated on energy, for fragments stopped in Si2. For a given isotopic pair, similar FoM values are found at all the employed bias voltages applied to Si2. This proves that the ΔE-E isotopic identification is not substantially affected by the partial depletion of Si2, provided that the signals, which become very slow, are suitably treated, as described in sect. 3.1.

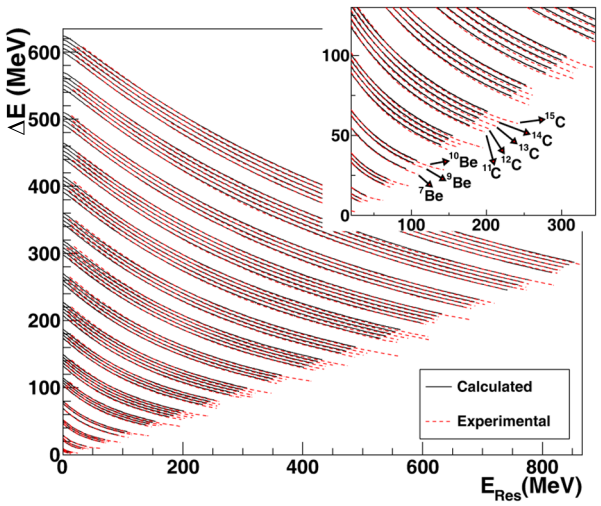

Fig. 4. (Color online) Comparison of the interpolation lines, manually drawn following the experimental isotopic ridges at 290 V, (dashed lines) with the curves obtained from energy loss calculations [26] (full lines). The inset shows a detail of the plot in the region of light elements.

Table 3. Figure of Merit (FoM) for adjacent peaks in a PID (Particle IDentification) spectrum. Events are integrated over all particle energies. The first column reports the selected isotopic pair, the other columns the associated FoM obtained at the different bias voltages applied to Si2. The number in parenthesis is the uncertainty associated with the least significant digit of the reported value.

Isotopes	Applied voltage (V)				
	105	130	200	235	290
^{6}Li-^{7}Li	1.51(9)	1.5(2)	1.4(1)	1.5(1)	1.5(1)
^{11}B-^{12}B	1.52(4)	1.50(6)	1.54(6)	1.43(6)	1.42(5)
^{12}C-^{13}C	1.50(5)	1.44(5)	1.50(6)	1.50(5)	1.51(6)
^{21}Ne-^{22}Ne	1.18(9)	1.21(6)	1.20(8)	1.18(3)	1.19(8)
^{24}Na-^{25}Na	1.10(2)	1.12(3)	1.11(3)	1.14(3)	1.16(8)
^{25}Mg-^{26}Mg	1.03(7)	1.1(1)	1.12(8)	1.08(7)	1.1(1)
^{29}Si-^{30}Si	0.98(3)	0.98(3)	0.92(3)	0.99(3)	0.97(3)
^{33}S-^{34}S	0.63(6)	0.74(9)	0.98(7)	0.69(9)	0.78(8)

3.3 Energy calibration

A usual calibration technique for ΔE-E telescopes exploits the so-called "punch-through" points of different isotopes (see ref. [28] sect. 3.2 or ref. [13] sect. 2.2). These are the points with the largest residual energy E_{RES} of each ΔE-E curve. Punch-through points in ADC units (ADU) have been estimated by visually inspecting the ΔE-E correlations in the punch-through region and the error on these values has been estimated to be usually less than 1% for ΔE and 1–2% for E_{RES}. From energy-range tables like [26] it is then possible to associate the proper deposited energies to the uncalibrated values. For each silicon detector, 37 punch-through points (for different isotopes with $2 \leq Z \leq 16$) have been used in order to calibrate the energy scale. A simple proportionality between ADC units and MeV has been assumed, as in previous FAZIA experiments. Table 4 summarizes the calibration fit results for Si2 at the different bias voltages. The calibration factor (second column of table 4) is determined with an uncertainty of less than 0.1% and it decreases steadily, for Si2, going from 105 to 290 V. However, it changes at most by 2% from the lowest to the highest applied voltage.

Table 4. First four columns: applied voltages, calibration factors, associated χ^2 and reduced χ^2 values for Si2. In all cases, the number of degrees of freedom (DoF) is 36. The standard deviation of the reduced χ^2 is 0.24. Last two columns: relative difference of calibration factors with respect to 290 V bias and estimated Si-equivalent entrance dead-layer (see sect. 3.3).

Voltage on Si2 (V)	Conv. Factor $\left(\frac{\mathrm{MeV}}{\mathrm{a.u.}}\right)$	χ^2	$\chi^2_R = \chi^2/\mathrm{DoF}$	$\delta_{290\,\mathrm{V}}$ %	Si-eq. dead layer (μm)
105	0.1962	34.5	0.96	2.03	17
130	0.1949	33.9	0.94	1.35	11
200	0.1937	26.3	0.73	0.73	6
235	0.1930	16.7	0.46	0.36	3
290	0.1923	24.3	0.68	–	0

From the reduced χ^2 values (fourth column of table 4) a reasonable agreement of the data with the assumed proportionality can be inferred. Since χ^2 increases from 290 V to 105 V, a small deviation from the assumed proportional law is suspected to be present at the lowest voltages.

In the undepleted region one expects a very low, if not zero, electric field. Therefore, apart from the slowing down of charge collection already shown in fig. 2, one would also expect a reduction in collection efficiency with respect to full depletion. While the general slowing down of charge collection is substantially confirmed (see also sect. 3.5), the reduction in collection efficiency (reported in the fifth column of table 4) seems to be at most $\sim 2\%$ at the lowest bias voltage. This value points to a high collection efficiency from the undepleted region. However, the calibration factors were obtained exploiting particle tracks extending over the whole detector thickness. Particles with shorter range will be addressed in sect. 3.4.

We remind that it is essential to use very long shaping times and to apply pole-zero cancellation of preamplifier decay (see sect. 3.1) to achieve such a result. Otherwise one observes the well-known ballistic deficit, an effect related to electronics and independent of charge collection efficiency [23,24]. On the other hand, ballistic deficit cannot explain the observed 2% variation of the calibration factor, since it has been estimated to be less than 0.5% (see sect. 3.1).

One can convert the observed dependence of the calibration factors on bias voltage into a Si-equivalent effec-

tive dead layer at the entrance side. Assuming a zero dead layer at 290 V, we calculated the dead layer thicknesses which would give the observed calibration factor at the other bias voltages. They are reported in the rightmost column of table 4. However, a real dead layer at the entrance of Si2 would affect not only the measured energies at the punch-through in Si2: to reach the active region of Si2, a particle would need a higher incident energy and, as a consequence, it would deposit a lower energy in Si1, thus lowering the ordinate of the leftmost point of the ΔE-E curve. That energy in Si1, which is easily derived by inspection of the ΔE-E correlations, is practically the same for all the employed biases and it is not compatible with the dead layer thickness quoted in table 4. In fact, a reduction of several MeV should be observed in presence of a dead layer of the estimated thickness. For example, a dead layer of 17 μm Si-equivalent estimated at 105 V would result in a reduction of about 10 MeV for the energy deposited in Si1 by a ^{10}B, while that value stays constant within 1 MeV. It is therefore possible to exclude the presence of a totally inactive layer at the entrance of Si2.

3.4 Energy response of ions as a function of the bias voltage

The results of sect. 3.3 showed that for particle tracks extending over the whole detector thickness the "end points" of each ΔE-E curve are stable in amplitude, within 2%, as a function of the bias voltage. A deeper investigation was devoted to studying the detector response in the whole energy range spanned by the ΔE-E correlations. To avoid systematic effects due to the energy loss calculations, we compare the charge-signal amplitude at different bias voltages with that at full depletion (taken as a reference), being the signal amplitude directly related to the collection efficiency. The detector response for each specific fragment type can be derived, thanks to the isotopic identification allowed by the ΔE(Si1) *vs.* $E_{\rm RES}$(Si2) correlations (see sect. 3.2).

For a given identified isotope, the events have been classified in bins of ΔE(Si1). Bins having the same ΔE(Si1), though taken at different bias voltages applied to Si2, correspond to the same incident energy (and to the same range in Si2, for a given A and Z). As a consequence, they also correspond to the same value of $E_{\rm RES}$ physically deposited in Si2: charge amplitudes recorded for such events are thus directly comparable.

Panel a) of fig. 5 shows, as a function of estimated particle range, the amplitude difference in ADC units (ADU)

$$\delta\mathcal{A} = \mathcal{A}_{\rm Si2}(290\,{\rm V}) - \mathcal{A}_{\rm Si2}(105\,{\rm V}).$$

The same difference is also reported in panel b) as a percentage of the value of $\mathcal{A}_{\rm Si2}(290\,{\rm V})$. Data refer to a few nuclear species, namely ^{4}He, ^{6}Li, ^{12}C and ^{17}O. Similar results are obtained at a bias voltage of 130 V (not shown); only the absolute and relative differences are reduced by about a factor of 2. At a bias of 200 V or greater, the difference $\delta\mathcal{A}$ has been found compatible with zero within the errors.

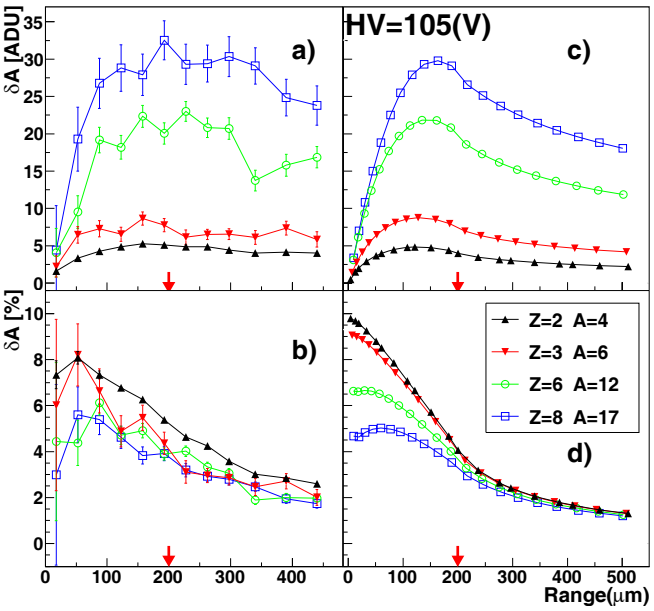

Fig. 5. (Color online) Panel a): experimental amplitude difference (ADC units) between events at 290 V and events at 105 V bias voltage as a function of particle range (estimated using the ΔE information from Si1). Data refer to four different isotopes: ^{4}He, ^{6}Li, ^{12}C and ^{17}O. Panel b): same data as in panel a) except that the amplitude difference is given as a percentage of the amplitude at 290 V. Panel c) calculated difference in the total collected charge, to be compared with the data in panel a) (see sect. 3.4 for details). Panel d) same values as in panel c), reported as a percentage of the total collected charge for comparison with panel b). The undepleted region is 200 μm thick: this value is evidenced by the arrow in each panel. The error bars refer to the statistical uncertainties.

The range, *i.e.* the penetration depth in the detector, revealed itself as the most relevant parameter to study the detector response. As a matter of fact, the amplitude difference at the two lowest biases increases up to a range approximately equal to the undepleted zone thickness (evidenced by the arrow) for all fragments. After that point, the difference remains about constant or slightly decreases. Relative differences of at most 8% (cf. ^{4}He at 105 V, fig. 5 panel b)) can be noticed.

As expected, for ranges of the order of the detector thickness the relative difference (fig. 5, panel b)) reaches the values obtained from the calibration factors in table 4 for the same bias voltages (2% for 105 V).

A detailed theoretical study of the collection process would be well beyond the aim of the present paper. Realistic numerical simulations, as those presented in [29–32], would be an ideal tool for such a study. Here we simply attempt an empirical description, trying to explain the experimental data by assuming incomplete charge collection from the undepleted region. The measured amplitude is proportional to the collected charge. The charge carri-

ers per unit thickness along the track are proportional, as a function of the penetration depth x, to the Bragg curve for the given fragment. Therefore, the contribution to the final amplitude coming from a given segment of the track is proportional to the integral of the Bragg curve over the same interval. To take into account the incomplete charge collection, each segment of the Bragg curve should be weigthed by an "efficiency factor". We ideally divide the detector into a depleted and an undepleted region and we apply different efficiency factors to the two regions, assuming 100% efficiency in the depleted region. It is apparent that a constant collection efficiency across the undepleted region cannot explain the data of fig. 5 panel b). In fact, for particles stopped in the undepleted region, it would give a constant relative difference independent of particle range. Assuming a variable collection efficiency $\eta(x)$, the simplest hypothesis is that of a linear variation with the distance x from the entrance surface, starting at some $\eta(0) < 1$ value and reaching $\eta(d) = 1$ where d is the thickness of the undepleted region ($\eta = 1$ all over the depleted region). Moreover, fig. 5 shows that the charge collection is more efficient for heavier fragments, *i.e.* those having a higher ionization density for a given penetration depth. Therefore, we introduce a term dependent on the stopping power $|\mathrm{d}E/\mathrm{d}x|$ in the collection efficiency (assuming a linear dependence for the sake of simplicity), obtaining

$$\eta(x) = \begin{cases} \eta(0) + (1-\eta(0))\dfrac{x}{d} + \alpha \left|\dfrac{\mathrm{d}E}{\mathrm{d}x}(x)\right| \dfrac{d-x}{d}, & \text{if } x < d \\ 1, & \text{if } x \geq d \end{cases}.$$

For each fragment and each value of the range, the "measurable" deposited energy is obtained as

$$E = \int \left|\frac{\mathrm{d}E}{\mathrm{d}x}(x)\right| \eta(x)\mathrm{d}x.$$

Panels c) and d) in fig. 5 present the result of our calculation. Since the integral of the Bragg curve gives an energy, we have converted it to ADU, exploiting the calibration factors of table 4. A reasonable agreement with the experimental values has been obtained for $\eta(0) = 0.89$ ($\eta(0) = 0.92$) at 105 V (130 V) and $\alpha = 0.4\,\mu$m/MeV.

The presented phenomenological approach seems to contain the right ingredients to reproduce the experimental behaviour. It has not been obtained from first principles or a microscopic description of the charge collection process and it is thus unable to give us detailed physical information. However, it can be used to get an approximate value of the charge collection efficiency in the undepleted region. On the whole, one can say that a maximum collection deficit of about 10% in the undepleted region is compatible with the observed behaviour for all reported fragments at the two lowest bias voltages of 105 and 130 V while data at 200 and 235 V are compatible with a collection efficiency of about 100%. To conclude, a surprisingly high average collection efficiency from the undepleted region (90% or more) must be assumed to reasonably reproduce the data at the two lowest biases.

From the observed behaviour, assuming a linear energy response at full depletion, a non-linearity of the order of few % can be inferred. In principle, this effect could be corrected for by exploiting the very same data shown in fig. 5. A preliminary analysis shows that a simple second order polynomial correction permits to obtain the "full depletion" amplitude (*i.e.* the value which would be obtained at 290 V) from the experimental amplitude at lower bias voltage, once the fragment has been correctly identified using either the PSA or the ΔE-E technique. However, the coefficients of the polynomial are different for different isotopes and it is still not clear if they can be derived from a simple functional dependence on Z and A.

3.5 Pulse shape analysis

The PSA technique permits to identify particles stopped in one silicon detector from information delivered by that detector alone. PSA will thus allow to reduce the identification thresholds when applied to the first telescope stage in a physics experiment. All results presented in this section have been obtained with a veto condition on the CsI(Tl) detector to select particles stopped in the detector under test, which in this work is Si2. Two methods of PSA have been used, based on the two correlations "Energy *vs.* Charge rise-time" and "Energy *vs.* Current maximum". Both techniques had been already investigated within the FAZIA R&D program [12–14].

In the top row of fig. 6 the correlation "Energy *vs.* Charge rise-time" is shown for Si2 at four of the five bias voltages employed in this work, namely 105, 130, 200 and 290 V: isotopic separation is quite good at 105 V and it worsens with increasing bias voltage, eventually disappearing for an applied voltage greater than 200 V (the correlation at 235 V, not shown in the picture, is similar to that at 290 V). The span of the horizontal axis shows how the rise-time decreases from about 13 μs to less than 400 ns when going from 105 to 290 V bias voltage.

Already from the top row of fig. 6, one can get an estimate of the minimum energy for which isotopic separation is possible. For instance, a threshold of about 110 MeV can be inferred for carbon ($Z = 6$) both at 105 and 130 V.

The second PSA method is the so-called "Energy *vs.* Current maximum" technique. The bottom row of fig. 6 shows the correlation "Energy *vs.* Current maximum" for Si2 at the same voltages as the top row. A better performance of this technique with respect to the previous one can be inferred. However, as for the "Energy *vs.* Charge rise-time" correlation, the isotopic separation worsens with increasing bias voltage. A residual contamination of punching-through particles, not vetoed by the CsI for geometrical reasons (see sect. 2), is present. They form ridges approximately along the diagonal in the "Energy *vs.* Current maximum" correlation (from the bottom-left corner to the top-right one).

The isotopic discrimination limit can be quantitatively evaluated by means of the already defined FoM [27], after the "Energy *vs.* Charge rise-time" or the "Energy *vs.* Current Maximum" correlations have been linearized by

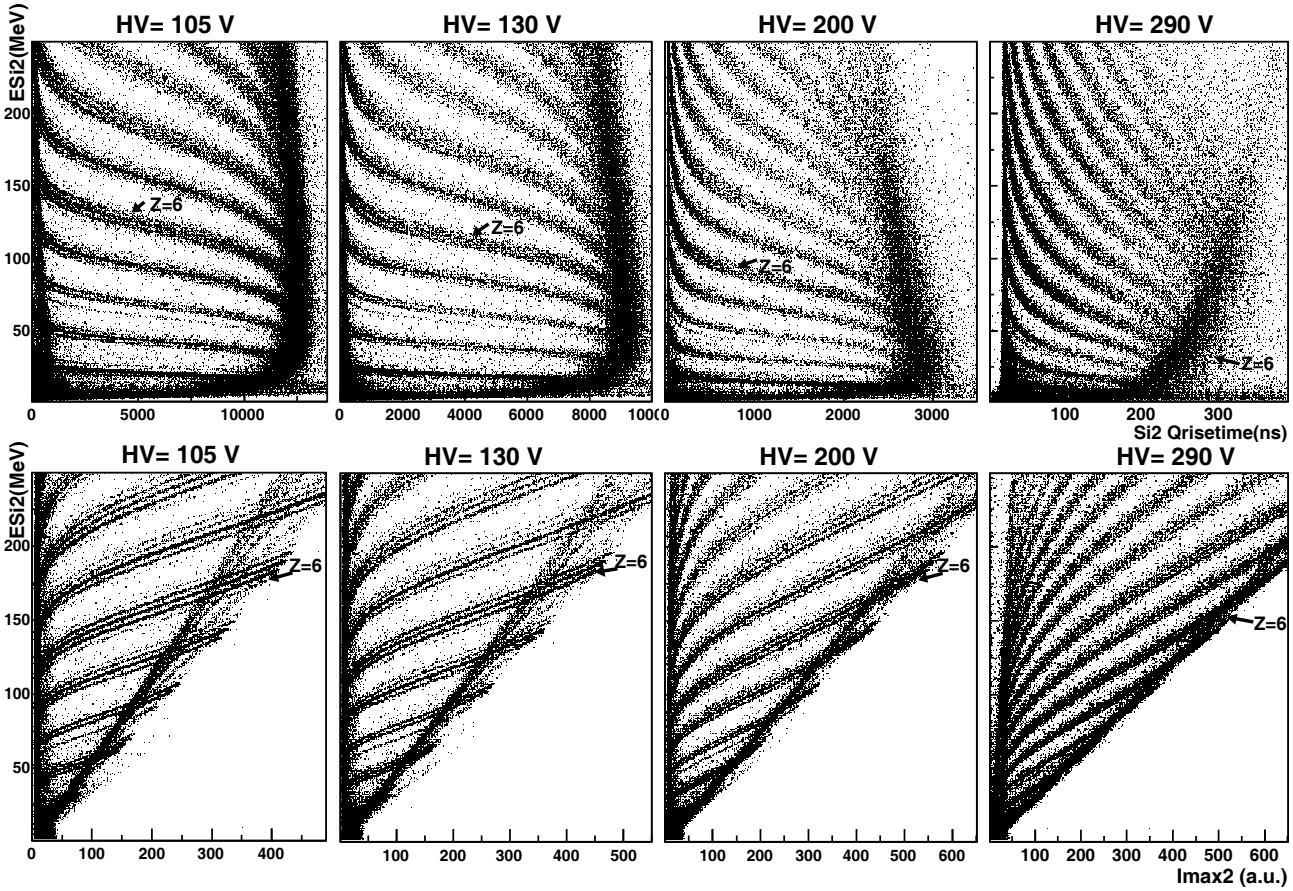

Fig. 6. Top: "Energy *vs.* Charge rise-time" correlations at different bias voltages. Bottom: "Energy *vs.* Current Maximum" correlations at the same bias voltages.

extracting a PID value, as already explained for ΔE-E in sect. 3.2. In this work we focus on the "Energy *vs.* Current Maximum" technique since it seems to perform better than the "Energy *vs.* Charge rise-time" one. In fact, FoM values extracted from "Energy *vs.* Current maximum" correlations, are higher than those obtained from the "Energy *vs.* Charge rise-time" method.

Figure 7 shows the FoM obtained from "Energy *vs.* Current maximum" correlations as a function of the particle range. We consider two isotopes as well separated if FoM is greater than 0.7 (see ref. [12]), corresponding to a peak-to-valley ratio of 2 when the two peaks are equal. For each isotopic pair a minimum penetration depth for which FoM > 0.7 can be inferred from graphs like those shown in fig. 7: it constitutes the lower threshold, in range, for isotopic identification. Such thresholds are shown in table 5 for various isotopic pairs at the different bias voltages. The corresponding incident energy is also reported. Figure 7 also shows that in a few cases the FoM value decreases for higher penetration, thus falling below the FoM $= 0.7$ line: for those cases we give range (and energy) intervals for good separation instead of a lower threshold. The expectation that the penetration depth is a more useful parameter than energy is confirmed by the fact that the identification thresholds (crossing of FoM $= 0.7$) in range are about the same for all Z values at a given bias voltage. The energy thresholds are found in good agreement with those visually estimated from the "Energy *vs.* Current Maximum" correlations. We notice that at 105 V and 130 V bias voltage the "Energy *vs.* Current maximum" method permits isotopic separation up to Al and Mg isotopes, respectively. In comparison, the "Energy *vs.* Charge rise-time" method only allows isotopic separation up to F (at 105 V) or C (at 130 V).

One also notices that no isotopic identification is obtained for fragments stopped in the undepleted region, *i.e.* the FoM crosses 0.7 for range values greater than the undepleted layer thickness. As a matter of fact, a rapid transition from a slow to a fast regime of charge collection can be recognized for all fragments as soon as they get close to the depleted region. This is particularly evident from the "Range *vs.* Charge rise-time" correlations of fig. 8, which refer to all fragments with $Z > 2$. It is interesting to see that the different ridges of fig. 6, top, tend to collapse on a single ridge when on the y-axis the fragment range is reported instead of the energy. Moreover, the rise-time stays approximately constant for range values within the undepleted region and it starts decreasing at a higher rate as soon as particles reach the depleted region, *i.e.* the region of non-zero electric field. This could be a signature of *field-enhanced funneling* [33–36], an extension of the electric field into the undepleted region along the ion track, which can produce a faster charge collection. A deeper study of this effect is planned by the FAZIA Collaboration.

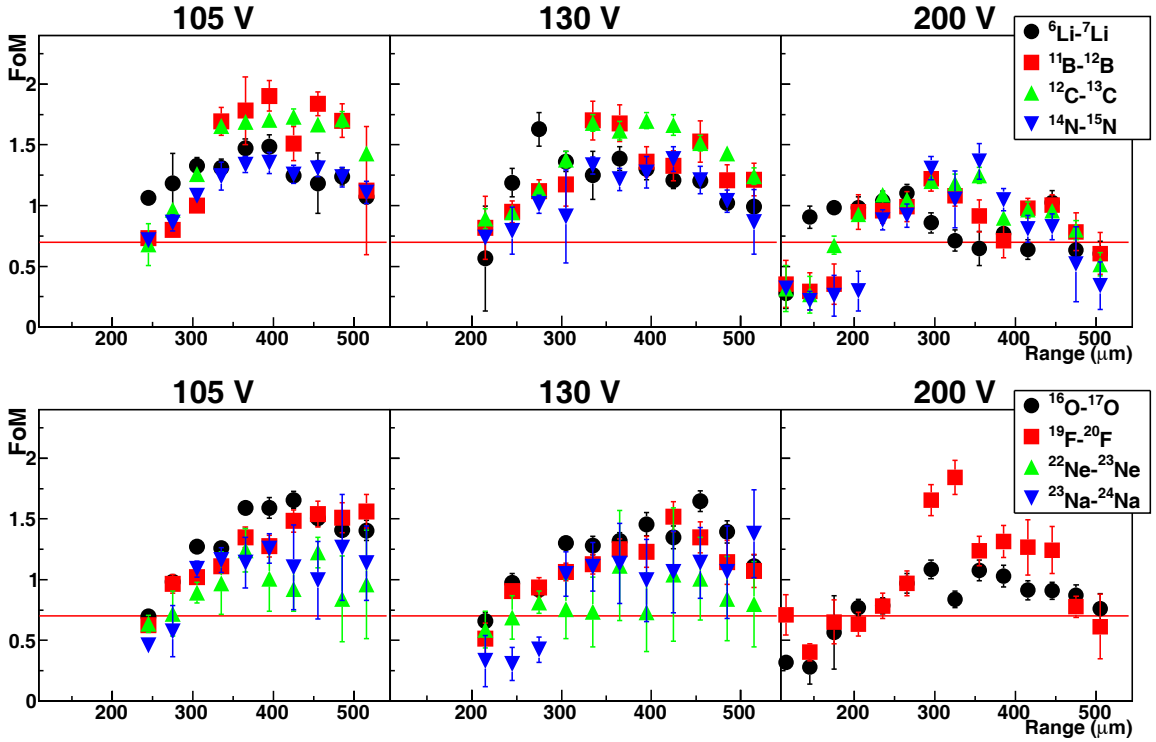

Fig. 7. (Color online) Isotopic identification with PSA using the "Energy *vs.* Current maximum" correlation. The FoM is shown for several isotopic pairs at 105, 130 and 200 V bias voltage as a function of particle range.

Table 5. Range and energy intervals for which good isotopic identification (*i.e.* FoM > 0.7) is achieved. Data refer to selected isotopes with $3 \leq Z \leq 13$ and to three applied voltages: 105, 130 and 200 V. A single value is reported when isotopic separation is achieved for stopped fragments of all ranges/energies above the low threshold. No value is reported when FoM < 0.7 for all range/energies at the given bias voltage.

	105 V		130 V		200 V	
Isotopes	Range (μm)	Energy (MeV)	Range (μm)	Energy (MeV)	Range (μm)	Energy (MeV)
^{6}Li-^{7}Li	240-	40-	220-	40-	130-	30-
^{10}B-^{11}B	240-	90-	220-	90-	170-	75-
^{12}C-^{13}C	250-	120-	220-	110-	180-	100-
^{14}N-^{15}N	250-	150-	220-	140-	200–480	130–225
^{16}O-^{17}O	250-	190-	220-	170-	220–470	170–270
^{19}F-^{20}F	250-	230-	230-	215-	230–470	215–335
^{22}Ne-^{23}Ne	260-	280-	240-	260-	240–390	260–355
^{23}Na-^{24}Na	270-	320-	290–400	335–410		
^{26}Mg-^{27}Mg	280-	380-	310–380	400–460		
^{27}Al-^{28}Al	320–410	455–530				

In the spirit of fig. 17 of ref. [13], the isotopic identification threshold in terms of deposited energy is plotted as a function of Z in fig. 9 for the elements without an upper energy threshold in table 5. Different symbols in fig. 9 correspond to different bias voltages, namely 105 V (empty squares), 130 V (empty circles) and 200 V (empty triangles). In the same picture, for the sake of comparison, the energy threshold for isotopic identification as given by the ΔE-E technique for a 311 μm thick ΔE detector (*i.e.* the minimum energy needed for the particle to punch through Si1 and to deposit some energy in Si2) is plotted as full triangles. As already shown in table 5, the threshold for mass identification increases for decreasing bias voltage.

For what concerns the charge identification, we will not deal with FoM values because a visual inspection of the "Energy *vs.* Current maximum" correlations is sufficient to determine the energy thresholds. From fig. 6, bottom row, it is apparent that at 105 V and 130 V bias voltage the energy threshold for charge identification is slightly lower than that for mass identification. This energy threshold

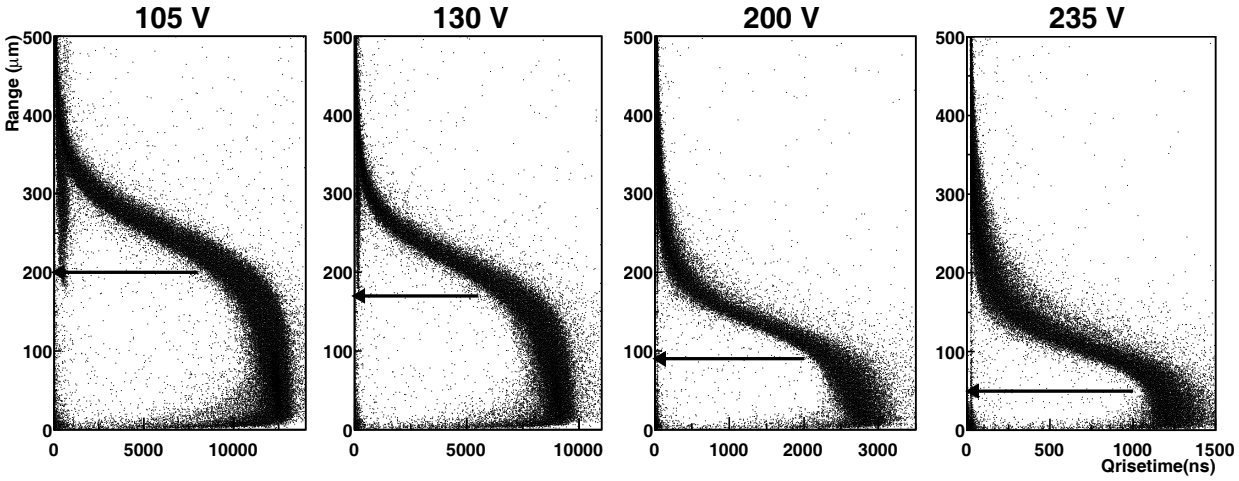

Fig. 8. "Range *vs.* Charge rise-time" correlations at 105, 130, 200 and 235 V for fragments with $Z > 2$. The arrows point to the estimated thickness of the undepleted region.

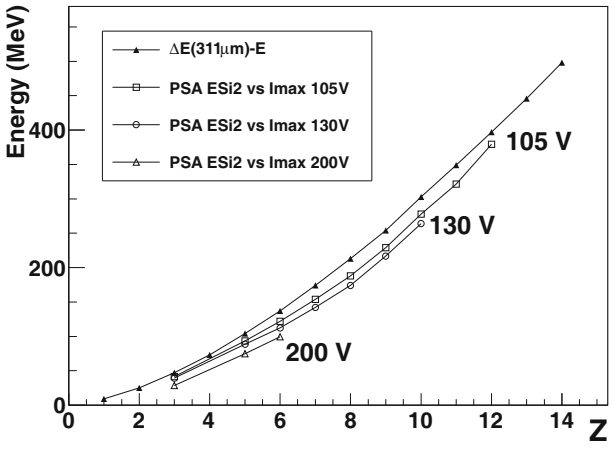

Fig. 9. Energy thresholds for isotopic identification at various bias voltages: 105 V (empty squares), 130 V (empty circles) and 200 V (empty triangles). The energy threshold for isotopic identification as given by the ΔE-E technique for a 311 μm thick ΔE detector is also plotted (full triangles).

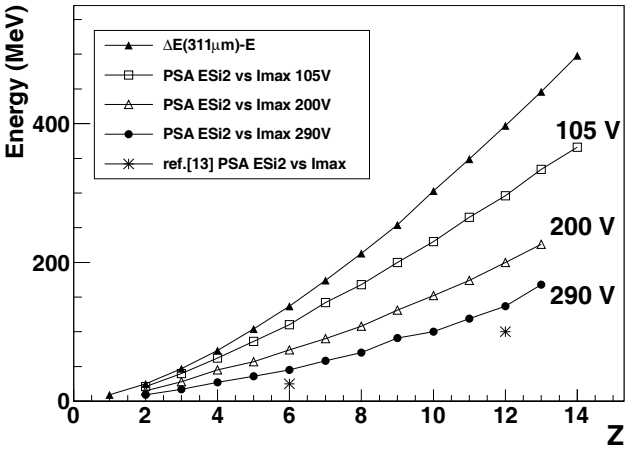

Fig. 10. Charge identification thresholds estimated from visual inspection of the "Energy *vs.* Current maximum" correlations for a bias voltage of 105 (empty squares), 200 (empty triangles) or 290 V (full circles). Thresholds affecting the ΔE-E technique are also shown as full triangles for a 311 μm thick detector. Values from a previous FAZIA work (ref. [13]) are also plotted (stars, see text).

for charge identification, shown in fig. 10 at bias voltages of 105, 200 and 290 V for $Z = 2$–13, becomes higher when reducing the bias voltage. This indicates that the better isotopic identification at low bias is achieved at the price of higher charge identification thresholds. In order to compare the present results with those obtained by the collaboration in previous experiments, we also show the identification thresholds as reported in [13] for the "Energy *vs.* Current maximum" method (stars). Since those data were obtained with a fully depleted detector, it is no surprise that the present result at full depletion gets quite close to the previous data. However, the thresholds in [13] were slightly lower and this could be due to the different doping uniformity (better than 1% in [13], only 6% for the present detector)[1].

[1] The different thickness of the detectors (306 μm in [13], 510 μm in the present work) should make no significant difference, according to the previous FAZIA experience.

4 Conclusions

A study of the response of a 500 μm thick n-TD Si detector, mounted as the second stage of a Si-Si-CsI telescope and biased at a voltage below that necessary to obtain full depletion, has been presented. The study takes into account both the energy response and the PS response of the detector.

For particles with a range equal to the detector thickness, the charge collection changes just by 2% between 105 V (60% depletion) and 290 V (full depletion) bias voltage. A remarkably high charge collection efficiency (about 90% or more) from the undepleted region of the detector is obtained, provided that pole-zero cancellation is applied and that signals are treated with a suitably long shaping time of a few tens of μs. The charge amplitude response of

the detector has been found linear within few % even at 105 V, when the undepleted region is 200 μm thick. Non-linearities of the order of 5–8% in the amplitude-energy response have been noticed for particles stopped in the undepleted region at 105 V bias voltage. These non-linearities can be corrected for, knowing the particle atomic and mass number, by using a simple second-order polynomial correction whose coefficients, however, are different for different ion types.

The ΔE-E performance is not affected by the incomplete depletion even when 40% of the wafer is not depleted.

The detector under test did not allow isotopic identification via PSA when biased at full depletion voltage. In fact its doping uniformity is only about 6%, while previous tests performed by the collaboration showed that a doping uniformity of about 1% FWHM or better is needed for isotopic identification [12]. It is not easy for manufacturers to provide ingots of $\approx$ 1% doping uniformity. The present result shows that it is still possible to get isotopic identification with PS techniques from detectors of worse doping uniformity. Underbiasing the first stage of a ΔE-E telescope, one can get isotopic identification at lower energy than with the ΔE-E technique alone. However, with respect to a good uniformity Si detector, the better isotopic resolution comes at the price of somewhat higher charge identification thresholds. Therefore, for experiments requiring an isotopic identification of fragments, either a comprimise must be found between the two conflicting requirements or the beam time should be partly devoted to measurements at low detector bias.

The long shaping times necessary for partially depleted detectors could impose the acquisition of relatively long signals (7000 samples in the present case). One could avoid memory or time limitations by employing decimation [37] after sampling, thus reducing the number of samples which must be acquired and processed. Pile-up issues could still limit the use of this technique at high counting rates, but the low beam currents at Radioactive Beam facilities should pose no such problems.

The authors would like to thank the LNS Superconducting Cyclotron staff, in particular D. Rifuggiato, for providing a very high-quality beam. The support of the Machine shop teams of LNS, of the Physics Departments of Florence (in particular M. Falorsi), of the Physics Departments of Naples and of the Physics Departments of Bologna (in particular M. Guerzoni and S. Serra) is gratefully acknowledged. The effective collaboration of the Physics Department of Florence (and in particular of E. Scarlini), of IPN (Orsay) and of LPC (Caen) is gratefully acknowledged. We also thank A. Boiano, A. Meoli and G. Tortone (INFN, Naples) for their invaluable assistance. Thanks are also due to N. Zorzi of FBK(Trento) for cooperative support in detector development. The research leading to these results has received funding from the European Union Seventh Framework Program FP7/2007-2013 under Grant Agreement n^{o} 262010 - ENSAR and from grants of Italian Ministry of Education, University and Research under contract PRIN 2010-2011.

References

1. INDRA Collaboration (E. Galichet *et al.*), Phys. Rev. C **79**, 064614 (2009) doi:10.1103/PhysRevC.79.064614.
2. T.X. Liu *et al.*, Phys. Rev. C **76**, 034603 (2007) doi:10.1103/PhysRevC.76.034603.
3. M. Di Toro *et al.*, Eur. Phys. J. A **13**, 155 (2002) doi:10.1140/epja1339-28.
4. Ad.R. Raduta, F. Gulminelli, Phys. Rev. C **75**, 044605 (2007) doi:10.1103/PhysRevC.75.044605.
5. J. Pouthas *et al.*, Nucl. Instrum. Methods A **357**, 418 (1995) doi:10.1016/0168-9002(94)01543-0.
6. S. Aiello *et al.*, Nucl. Phys. A **583**, 461 (1995) doi:10.1016/0375-9474(94)00705-R.
7. A. Moroni *et al.*, Nucl. Instrum. Methods A **556**, 516 (2006) doi:10.1016/j.nima.2005.10.123.
8. S. Wuenschel *et al.*, Nucl. Instrum. Methods A **604**, 578 (2009) doi:10.1016/j.nima.2009.03.187.
9. D.A. Bromley, IRE Trans. Nucl. Sci. **9**, 135 (1962) doi:10.1109/TNS2.1962.4315986.
10. FAZIA Collaboration, `http://fazia2.in2p3.fr/spip`.
11. FAZIA Collaboration (R. Bougault *et al.*), Eur. Phys. J. A **50**, 47 (2014) doi:10.1140/epja/i2014-14047-4.
12. FAZIA Collaboration (L. Bardelli *et al.*), Nucl. Instrum. Methods A **654**, 272 (2011) doi:10.1016/j.nima.2011.06.063.
13. FAZIA Collaboration (S. Carboni *et al.*), Nucl. Instrum. Methods A **664**, 251 (2012) doi:10.1016/j.nima.2011.10.061.
14. FAZIA Collaboration (N. Le Neindre *et al.*), Nucl. Instrum. Methods A **701**, 145 (2013) doi:10.1016/j.nima.2012.11.005.
15. FAZIA Collaboration (G. Pasquali *et al.*), Eur. Phys. J. A **48**, 158 (2012) doi:10.1140/epja/i2012-12158-6.
16. M. Bruno *et al.*, Eur. Phys. J. A **49**, 128 (2013) doi:10.1140/epja/i2013-13128-2.
17. J.A. Dueñas *et al.*, Nucl. Instrum. Methods A **714**, 48 (2013) doi:10.1016/j.nima.2013.02.032.
18. FBK web site, `http://http://www.fbk.eu`.
19. FAZIA Collaboration (L. Bardelli *et al.*), Nucl. Instrum. Methods A **602**, 501 (2009) doi:10.1016/j.nima.2009.01.033.
20. FAZIA Collaboration (L. Bardelli *et al.*), Nucl. Instrum. Methods A **605**, 353 (2009) doi:10.1016/j.nima.2009.03.247.
21. H. Hamrita *et al.*, Nucl. Instrum. Methods A **531**, 607 (2004) doi:10.1016/j.nima.2004.05.112.
22. G. Pasquali *et al.*, Nucl. Instrum. Methods A **570**, 126 (2007) doi:10.1016/j.nima.2006.10.008.
23. B.E. Baldinger, W. Franzen, *Amplitude and Time Measurement in Nuclear Physics*, in *Advances in Electronics and Electron Physics*, Vol. **VIII** (Academic Press, 1955).
24. B.W. Loo, F.S. Goulding, D. Gao, IEEE Trans. Nucl. Sci. **NS-35**, 114 (1988) doi:10.1109/23.12686.
25. NUCL-EX Collaboration (L. Bardelli *et al.*), Nucl. Instrum. Methods A **560**, 524 (2006) doi:10.1016/j.nima.2005.12.250.
26. F. Hubert *et al.*, At. Data Nucl. Data Tables **46**, 1 (1990) doi:10.1016/0092-640X(90)90001-Z.

27. R.A. Winyard, J.E. Lutkin, G.W. McBeth, Nucl. Instrum. Methods **95**, 141 (1971) doi:10.1016/0029-554X(71)90054-1.
28. B. Braunn *et al.*, Nucl. Instrum. Methods B **269**, 2676 (2011) doi:10.1016/j.nimb.2011.08.010.
29. NUCL-EX Collaboration (L. Bardelli *et al.*), in *Proceedings of the International Workshop on Multifragmentation IWM2005* (2005).
30. Z. Sosin, Nucl. Instrum. Methods A **693**, 170 (2012) doi:10.1016/j.nima.2012.07.020.
31. M. Pârlog *et al.*, Nucl. Instrum. Methods A **613**, 290 (2010) doi:10.1016/j.nima.2009.12.010.
32. H. Hamrita *et al.*, Nucl. Instrum. Methods A **642**, 59 (2011) doi:10.1016/j.nima.2011.03.053.
33. C.-M. Hsieh *et al.*, IEEE Trans. Electron Devices **ED-30**, 686 (1983).
34. J.A. Zoutendyk, C.J. Malone, IEEE Trans. Nucl. Sci. **NS-31**, 1101 (1984).
35. H.L. Grubin *et al.*, IEEE Trans. Nucl. Sci. **NS-31**, 1161 (1984).
36. F. Fontanelli *et al.*, Nucl. Instrum. Methods A **269**, 603 (1988).
37. Alan V. Oppenheim, Ronald W. Schafer, *Discrete-Time Signal Processing* (Pearson, 2010).